Article

Cell Reports

# The RNA Binding Protein IMP2 Preserves Glioblastoma Stem Cells by Preventing let-7 Target Gene Silencing

## Graphical Abstract

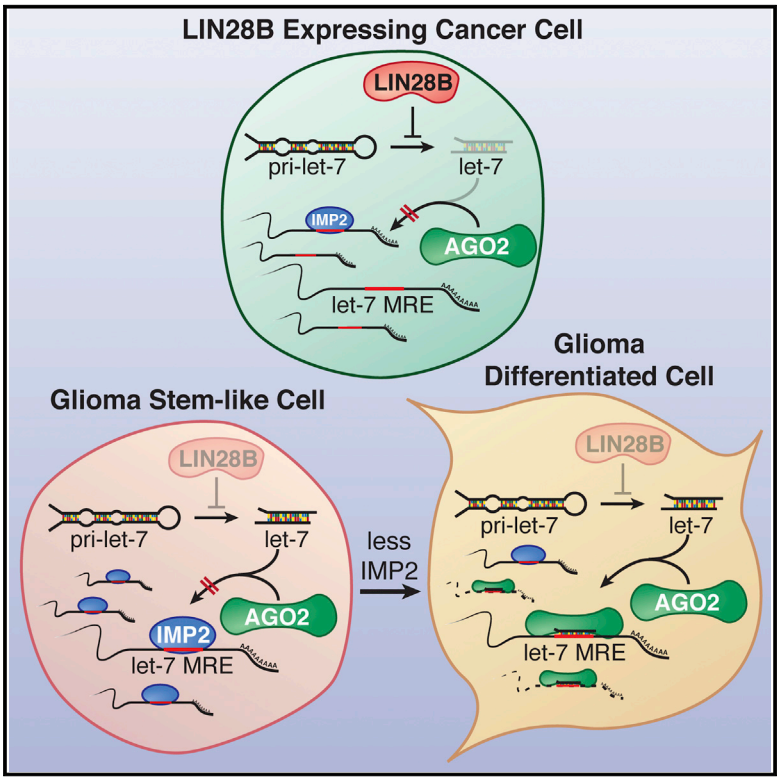


## Highlights

- GBM stem cells (GSCs) express let-7 miRNAs and their target genes in the absence of LIN28
- The RNA-binding protein IMP2, a let-7 target, is highly expressed in GSCs
- PAR-CLIP reveals that IMP2 binds let-7 target genes preventing their silencing
- IMP2 may substitute for LIN28 in let-7 target gene protection and GSC preservation

## Authors

Nils Degrauwe, Tommy B. Schlumpf, Michalina Janiszewska, ..., Mario-L. Suvà, Renato Paro, Ivan Stamenkovic

## Correspondence

ivan.stamenkovic@chuv.ch

## In Brief

Glioblastoma stem cells express elevated levels of let-7 miRNAs as well as their target genes, including *IMP2*. Degrauwe et al. show that the RNA-binding protein IMP2 binds to let-7 recognition elements on target transcripts, protecting them from degradation. IMP2 provides an alternative to LIN28B toward preserving glioblastoma stem cells.

## Accession Numbers

GSE73847

Degrauwe et al., 2016, Cell Reports *15*, 1634–1647
May 24, 2016 
http://dx.doi.org/10.1016/j.celrep.2016.04.086

OPEN ACCESS
CellPress

Cell Reports
Article

# The RNA Binding Protein IMP2 Preserves Glioblastoma Stem Cells by Preventing let-7 Target Gene Silencing

Nils Degrauwe,[1,7] Tommy B. Schlumpf,[2,7] Michalina Janiszewska,[3] Patricia Martin,[1] Alexandra Cauderay,[1] Paolo Provero,[4] Nicolo Riggi,[1] Mario-L. Suvà,[5,6] Renato Paro,[2,8] and Ivan Stamenkovic[1,8,*]

[1]Division of Experimental Pathology, Institute of Pathology, CHUV, Faculty of Biology and Medicine, University of Lausanne, Rue du Bugnon 25, 1011 Lausanne, Switzerland

[2]Department of Biosystems Science and Engineering, ETH Zürich, Mattenstrasse 26, 4058 Basel, Switzerland

[3]Department of Medical Oncology, Dana-Farber Cancer Institute and Department of Medicine, Harvard Medical School, Boston, MA 02215, USA

[4]Department of Molecular Biotechnology and Life Sciences, University of Turin, Turin 10126, Italy

[5]Department of Pathology and Center for Cancer Research, Massachusetts General Hospital and Harvard Medical School, Boston, MA 02114, USA

[6]Broad Institute of MIT and Harvard, Cambridge, MA 02142, USA

[7]Co-first author

[8]Co-senior author

*Correspondence: ivan.stamenkovic@chuv.ch

http://dx.doi.org/10.1016/j.celrep.2016.04.086

## SUMMARY

**Cancer stem cells (CSCs) can drive tumor growth, and their maintenance may rely on post-transcriptional regulation of gene expression, including that mediated by microRNAs (miRNAs). The let-7 miRNA family has been shown to induce differentiation by silencing stem cell programs. Let-7-mediated target gene suppression is prevented by LIN28A/B, which reduce let-7 biogenesis in normal embryonic and some cancer stem cells and ensure maintenance of stemness. Here, we find that glioblastoma stem cells (GSCs) lack LIN28 and express both let-7 and their target genes, suggesting LIN28-independent protection from let-7 silencing. Using photoactivatable-ribonucleoside-enhanced crosslinking and immunoprecipitation (PAR-CLIP), we show that insulin-like growth factor 2 mRNA-binding protein 2 (IMP2) binds to let-7 miRNA recognition elements (MREs) and prevents let-7 target gene silencing. Our observations define the RNA-binding repertoire of IMP2 and identify a mechanism whereby it supports GSC and neural stem cell specification.**

## SIGNIFICANCE

Human tumors are shaped by genetic evolution of cancer cells but also display superimposed hierarchies reminiscent of tissue development, where cancer stem cells (CSCs) can drive tumor growth and give rise to differentiated progeny. The mechanisms that underlie CSC emergence and ensure their maintenance are diverse, rendering their understanding key for designing therapeutic strategies aimed toward eliminating CSC properties or the cells themselves. We show that the RNA-binding protein IMP2 helps maintain glioblastoma stem cells by blocking the target gene silencing action of let-7 miRNA family members, which play a central role in abolishing stemness and promoting differentiation. Our observations elucidate a novel mechanism implicated in let-7 target gene protection and GSC maintenance that may be amenable to therapeutic targeting.

## INTRODUCTION

Glioblastoma (GBM) is the most common and the most lethal primary brain malignancy in adults, with a 5-year survival rate below 5%, despite aggressive multimodal therapy. Refractoriness to therapy is believed to reside in high intra-tumor heterogeneity resulting in part from hierarchical tumor cell organization (Patel et al., 2014). Glioblastoma contains highly plastic subpopulations of cells that are capable of self-renewal, tumor initiation, and differentiation into cells that constitute the tumor bulk, consistent with the functional definition of cancer stem cells (CSCs) (Kreso and Dick, 2014). These cells are commonly referred to as glioma stem cells (GSCs) and are thought to bear the principal responsibility for resistance to therapy and relapse (Singh et al., 2003; Chen et al., 2012; Bao et al., 2006). GSC plasticity is a product of epigenetic and post-transcriptional programs that determine cell hierarchies during normal development and neoplastic growth. Epigenetic modifications of DNA and chromatin, as well as post-transcriptional regulation of gene expression by non-coding RNAs, including microRNAs (miRNAs), underlie reprogramming of non-cancerous cells during development and tissue repair. The same mechanisms are believed to be responsible for the reprogramming that

accompanies transformation and drives CSC development. Although the complexity of epigenetic and post-transcriptional regulation of the genome precludes prediction as to which particular programs dominate CSC specification in different cancer types, the ability of miRNAs to fine-tune expression of entire gene networks places them among prime candidate contributors toward establishing and maintaining CSC properties.

miRNAs and RNA-binding proteins (RBPs) are expressed in a cell-type- and state-dependent fashion and constitute two essential regulators of mRNA stability. miRNAs are 21- to 22-nt non-coding RNAs that mediate post-transcriptional silencing by target mRNA degradation or translational repression (Bartel, 2009) and that are implicated in the regulation of virtually all biological processes in multicellular organisms (He and Hannon, 2004; Yu et al., 2007). Following transcription by RNA polymerase II, primary precursor miRNAs undergo sequential endonucleolytic cleavage by RNase III enzymes Drosha and Dicer in the nucleus and cytoplasm, respectively, to yield 21- to 22-nt double-stranded RNA (Lee et al., 2002). The duplex is then loaded onto the RNA-induced silencing complex (RISC), the core of which consists of Argonaute proteins (AGO1-4), and the passenger strand is unwound and removed leaving the guide strand to target transcripts for repression. Imperfect complementarity allows a single miRNA to target hundreds of mRNAs, many of which may function in concert to modulate cell fate transitions (Ivey and Srivastava, 2010). Alterations in global or selected miRNA biogenesis can therefore have a powerful impact on normal and cancer stem cell fate, as recently demonstrated in diverse cancer types (De Vito et al., 2012; Melo et al., 2010; Takahashi et al., 2014).

RBPs affect critical steps of posttranscriptional gene regulation, including mRNA maturation, splicing, translation, and stability (Gerstberger et al., 2014). Recent evidence suggests that a subset of RBPs can modulate miRNA-mediated mRNA silencing by binding sequences at or in close proximity to miRNA recognition elements (MREs) (reviewed in van Kouwenhove et al., 2011). However, only a few RBPs have been assigned oncogenic or tumor suppressive functions thus far (van Kouwenhove et al., 2011), and fewer still are known to play a relevant role in CSC biology. Notable exceptions are the oncofetal RBPs LIN28A/B (collectively referred to as LIN28), which are potent oncogenes expressed in embryonic stem cells and CSCs of several tumor types (Shyh-Chang and Daley, 2013; Nguyen et al., 2014) that selectively inhibit biogenesis of let-7, a 13-member tumor-suppressor miRNA family (Viswanathan et al., 2008, 2009; Heo et al., 2009). Let-7 miRNAs are highly evolutionarily conserved heterochronic genes, which in mammals regulate differentiation of, among others, embryonic stem cells (Viswanathan et al., 2008). Repression of let-7 family members by LIN28 is associated with normal stem cell maintenance and may participate in transformation as well as CSC emergence in diverse tumor types (Viswanathan et al., 2009; Nguyen et al., 2014). In the physiological context, the LIN28/let-7 axis operates to maintain either an embryonic stem cell or a differentiated state and may be exploited by tumor cells to modulate their own plasticity.

In this work, we interrogated the implication of miRNAs in primary GSC establishment and maintenance and found that the let-7 miRNA family and many of its target genes are highly expressed in both GSCs and their non-tumorigenic progeny. LIN28 was not detected in primary GBM cell cultures, suggesting that alternative, LIN28-independent mechanisms may contribute to preserve GSCs from let-7 tumor- and stemness-suppressive functions. We previously showed that the oncofetal RBP insulin-like growth factor 2 mRNA-binding protein 2 (IMP2), a canonical let-7 target, is highly expressed in GSCs and essential for their maintenance (Janiszewska et al., 2012). IMP2 belongs to a family of RBPs (together with IMP1 and IMP3) that are almost exclusively expressed during embryogenesis and involved in RNA localization, translation, and stability (Bell et al., 2013; Nielsen et al., 1999). IMPs are frequently re-expressed in diverse cancer types, where they may participate in invasion, metastasis, and CSC maintenance (Stöhr and Hüttelmaier, 2012; Janiszewska et al., 2012). Intriguingly, we found IMP2 to be co-expressed with several validated let-7 targets in GBM cells and therefore addressed the possibility that as an RBP, IMP2 may promote tumorigenicity and stemness in GBM by preventing let-7 target gene silencing.

Using photoactivatable-ribonucleoside-enhanced crosslinking and immunoprecipitation (PAR-CLIP) of IMP2 to identify RNA-RBP interactions with high resolution (Hafner et al., 2010), in primary proneural GSCs and their progeny, we show that IMP2 binds a subset of transcripts, including let-7 targets, directly on predicted MREs and protects them from miRNA-dependent silencing. Loss of clonogenicity and tumor-initiating capacity incurred by GSCs depleted of IMP2 was rescued by LIN28B, which restored expression of let-7 responsive transcripts. Similar to its effects in GSCs, IMP2 deletion repressed candidate let-7 target genes in sub-ventricular zone (SVZ) neural stem cells (NSCs) and impaired NSC clonogenicity in vitro. Our observations demonstrate that IMP2 helps specify GSC features in part by protecting let-7 family target transcripts from degradation and uncover a LIN28-independent mechanism shared by GSCs and NSCs that prevents let-7 target gene silencing.

## RESULTS

### Let-7 Family Members and Their Target mRNAs Are Highly Expressed in Primary GBMs

To identify candidate miRNAs that may be important in GSC specification, we assessed global miRNA levels in recently characterized primary GBM cells derived from three different patients (Wakimoto et al., 2012; Rheinbay et al., 2013; Suvà et al., 2014). GSCs can be propagated as spheroids (the terms spheroid and sphere will henceforth be used interchangeably) under serum-free conditions in vitro and phenocopy the parental tumor following xenotransplation into mice (Wakimoto et al., 2012). Upon exposure to serum, GSCs undergo transcriptional and post-transcriptional reprogramming that leads to differentiation, adhesion to substrate in vitro, and loss of tumor initiating capacity in vivo (Suvà et al., 2014). Cells obtained from freshly dissociated human tumors were grown as spheroids under serum-free conditions, with half of the culture being subsequently exposed to serum to generate adherent progeny (Figure 1A). Spheroid-derived cells from all three samples were highly tumorigenic in immunocompromised mice, forming tumors that recapitulated the histology of the original mass in vivo, whereas the adherent

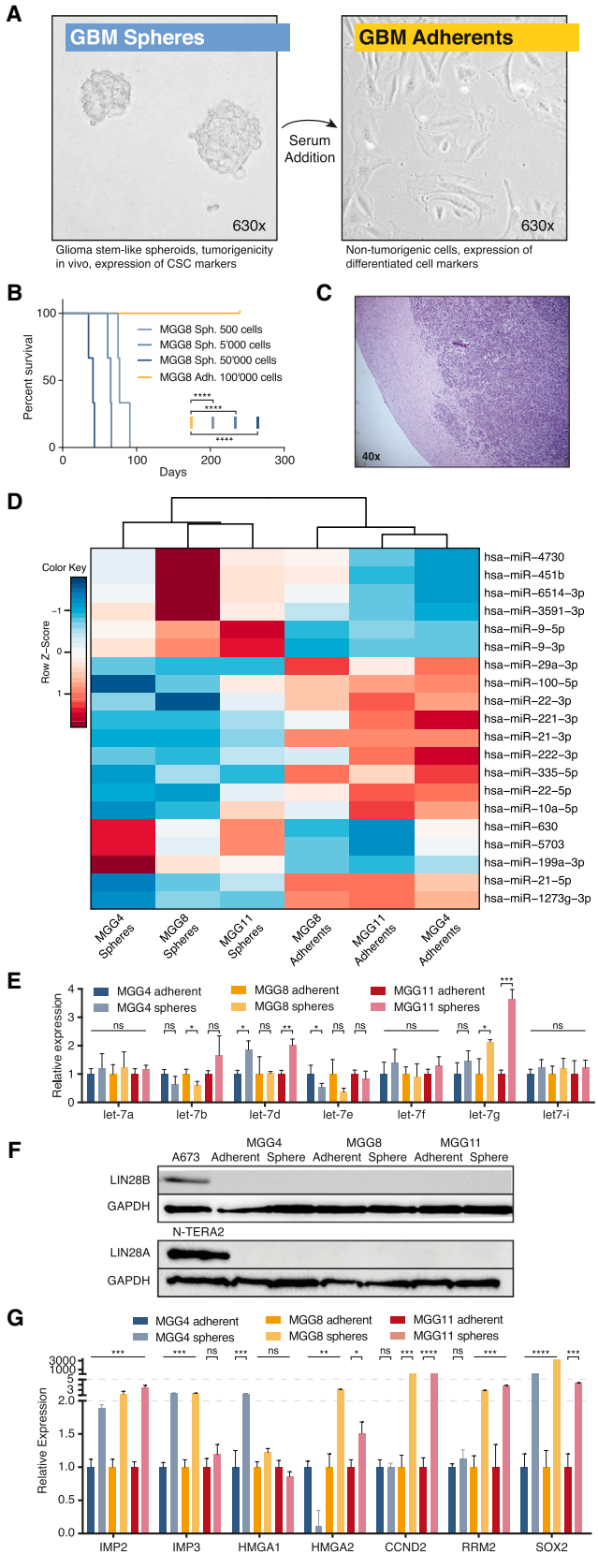


**Figure 1. GBM Sphere and Adherent Cell Properties**

(A) Representative image of primary tumor cultures and their signature properties. Glioma stem-cell-like enriched spheroids (left) and adherent cells grown as monolayers (right).

(B) Survival of mice injected with indicated numbers of sphere-derived and adherent MGG8 cells (three mice per condition). Statistical significance was calculated using log-rank test and is denoted as ****$p \leq 0.0001$.

(C) Representative histology of tumors formed by spheroid-derived cells.

(D) Hierarchical clustering of 20 miRNAs with highest fold change between GSC and adherent states of MGG4, 8 and 11 cells, as measured by miRNA microarrays. Color code indicates row *Z* score. Columns were reordered according to distance and rows according to clusters of similar expression.

(E) Relative expression of mature let-7 family miRNAs as assessed by qPCR and normalized to the respective adherent cell values. Data are presented as the mean ± SD. p values are denoted as ***$p \leq 0.001$, **$p \leq 0.01$, *$p \leq 0.05$, and ns (non-significant).

(F) WB of LIN28A and LIN28B in both cell states of all three primary GBM cultures. A673 Ewing sarcoma cells and N-TERA2 embryonal carcinoma cells were used as positive controls and GAPDH for equal loading assessment.

(G) Relative expression of a panel of validated let-7 target genes and SOX2 (a GSCs marker) as assessed by qPCR, normalized to respective adherent cell values. Data are presented as the mean ± SD. p values are denoted as ****$p \leq 0.0001$, ***$p \leq 0.001$, **$p \leq 0.01$, *$p \leq 0.05$, and ns (non-significant).

progeny failed to initiate tumor growth (Figures 1B and 1C; data not shown). A fraction of spheroid-derived cells expressed CD133 in vitro, a marker proposed to be associated with stem cell features in GBM (Bao et al., 2006) (Figure S1A), whereas adherent cells expressed markers of astrocytic and neuronal differentiation (Figure S1B). Microarray-based analysis of miRNA expression revealed that spheroids and adherent cells from different tumors clustered according to the cell state (Figure 1D). Subsequent qPCR validation of spheroid and adherent cell miRNA expression profiles confirmed robust upregulation in spheroids of miRNAs reported to be highly expressed in GSC-enriched $CD133^+$ GBM cells (Schraivogel et al., 2011) (Figure S1C).

Let-7 miRNA family members are repressed in embryonic stem cells and CSCs, primarily because of LIN28-dependent impairment of precursor maturation, which prevents let-7 target transcript degradation. Intriguingly, our microarray data and corresponding qPCR validation not only failed to reveal global repression of let-7 family miRNAs in GSCs compared to adherent cells but also showed let-7 family members to be among the most highly expressed miRNAs in both cell states (Figure 1E; Figure S1D). Consistent with this observation, neither LIN28A nor LIN28B was expressed in our GBM cells as assessed by western blot (WB) (Figure 1F) and qPCR analysis (Figure S1E), yet despite elevated let-7 expression, most validated let-7 targets were upregulated in GSCs compared to adherent cells (Figure 1G). We therefore addressed the existence of a LIN28-independent mechanism that may contribute to inhibition of let-7 tumor- and stemness-suppressive functions in GBM.

## Identification of the IMP2 Binding Repertoire in GBM with PAR-CLIP

A possible explanation for the expression of both let-7 family members and their target transcripts may lie in RBPs that operate through different mechanisms than that of LIN28. RBPs can protect transcripts from miRNA-dependent degradation by

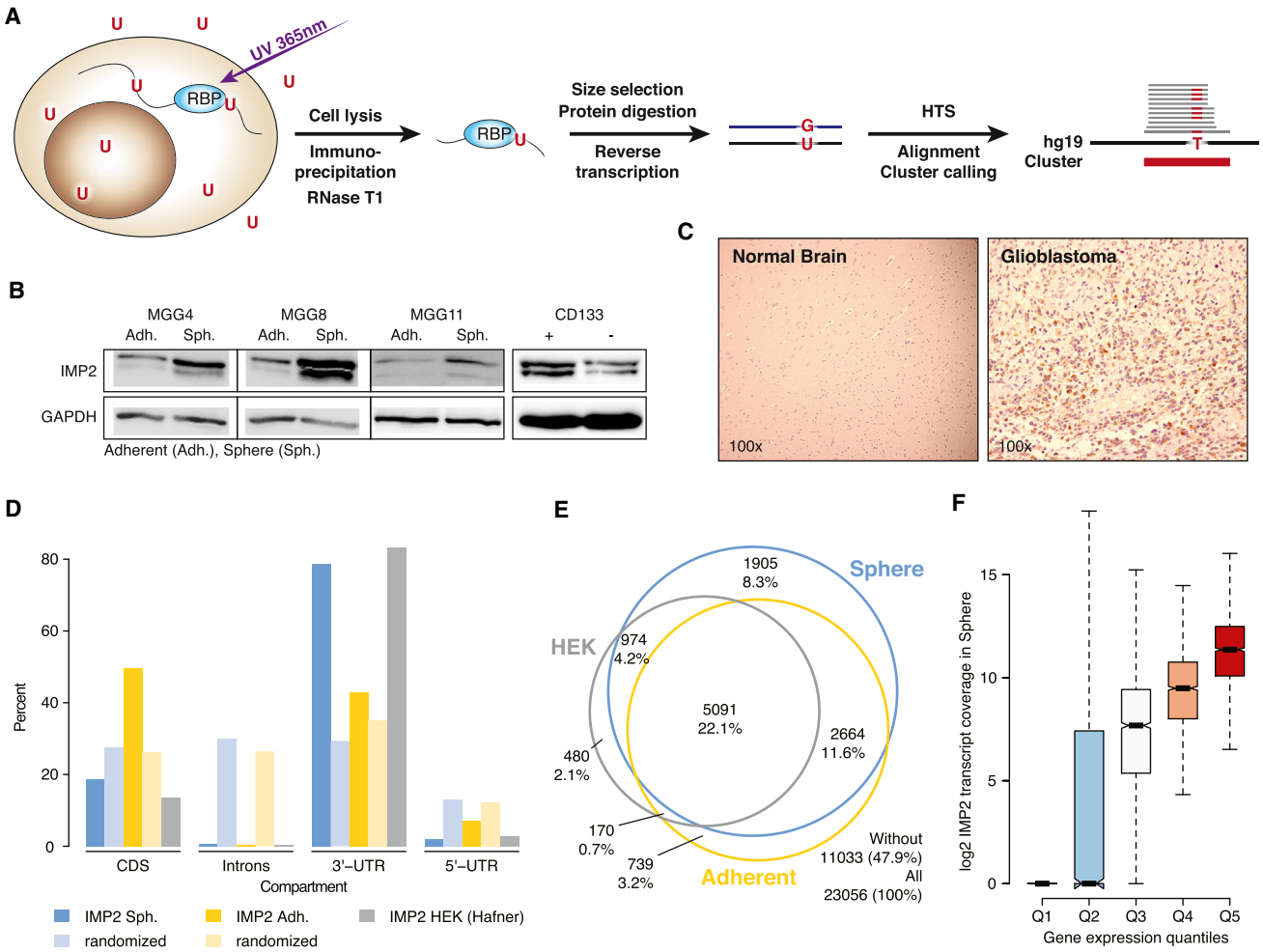


**Figure 2. PAR-CLIP of IMP2 in GBM Spheres and Adherent Cells**

(A) Overview of the PAR-CLIP procedure. Cells that have taken up 4-SU are crosslinked by 365-nm irradiation and the protein of interest immunoprecipitated. After SDS-PAGE, gel extraction, and proteinase K digestion of the protein-RNA complex, a library of bound RNAs is prepared and sequenced. Binding regions (clusters) are identified using the sequencing coverage and T-to-C nucleotide transition introduced by reverse transcription at crosslinked sites.

(B) WB of IMP2 in three primary GBM cultures and MGG8 spheres sorted for CD133 expression with GAPDH as a loading control.

(C) Immunohistochemistry using anti-IMP2 antibody on normal brain and GBM sections.

(D) Percentage of IMP2 clusters in spheres (blue) and adherent cells (yellow) localizing to the indicated gene regions. HEK293T IMP2 clusters (Hafner et al., 2010) and 10-fold randomization within genes are included for comparison.

(E) Overlap between genes bound by IMP2 in spheres, adherent cells, and HEK293T cells. The number of genes and fraction of the total are indicated within each overlap.

(F) Distribution of total IMP2 binding coverage for gene quantiles separated according to mRNA expression (2,216 genes each) for spheroids. See also Figure S2K for adherent cells.

binding directly to MREs of target mRNAs. Thus, IMP1 and IMP3 can counteract miRNA-mediated repression of *MITF* and *HMGA2* transcripts, respectively, by binding to their MREs (Goswami et al., 2015; Jønson et al., 2014). Importantly, numerous RBPs whose transcripts are themselves targets of a given miRNA protect their own transcript in addition to the other target mRNAs of the miRNA in question, thereby creating a positive feedback loop (Xue et al., 2013). It has been shown that IMP2, a validated let-7 target, is re-expressed in GBM and essential for GSC maintenance and survival, in part through regulation of GSC metabolism (Boyerinas et al., 2008; Janiszewska et al., 2012). Using TCGA glioblastoma database we found that *IMP2* is co-expressed with several canonical let-7 target transcripts, including *HMGA1*, *HMGA2*, *IMP1*, *IMP3*, and *ARID3B* (Figure S2A; data not shown). To address the putative role of IMP2 in miRNA target protection, we mapped its binding sites using PAR-CLIP, a cross-linking method that takes advantage of the incorporation of photoreactive ribonucleoside analogs into cells. UV irradiation followed by immunoprecipitation of the RBP of interest coupled to deep sequencing allows transcriptome-wide identification of the binding sites (Figure 2A). In addition, T-to-C conversion in cDNAs at crosslinked nucleosides

delineate binding regions with high accuracy and allow their discrimination from background RNA (Hafner et al., 2010).

IMP2 was expressed in both GSC-enriched spheroids and their adherent progeny, but expression was markedly higher in the former (Figure 2B). Accordingly, sphere-derived CD133$^+$ cells displayed higher IMP2 expression than their CD133$^-$ counterparts (Figure 2B; Figure S2B). IMP2 was undetectable in normal adult brain sections (Figure 2C), marginally expressed in normal human astrocytes, and strongly expressed in GBM (Figure S2C). Interrogation of The Cancer Genome Atlas (TCGA) database revealed robust IMP2 expression in all GBM subtypes, with some minor variations (Figure S2D). Importantly, depletion of IMP2 in GSCs by short hairpin RNA (shRNA) strongly impaired their proliferation and self-renewal (Figures S2E and S2F).

Two biological replicates of IMP2 PAR-CLIP were conducted in both highly tumorigenic GSC-enriched spheroids and their non-tumorigenic adherent progeny derived from the MGG8 primary tumor (Rheinbay et al., 2013), a GBM of the proneural subtype where elevated expression of *IMP2* has a negative prognostic value (Janiszewska et al., 2012). RNA corresponding to both IMP2 isoforms was pooled (Figure S2G), and we identified 167,278 and 70,451 binding regions (clusters) in both replicates of spheres and adherent cells, respectively. The number of binding sites per gene correlated well between the replicates (Pearson spheres [Sph] 0.93, adherent [Adh] 0.86; Figure S2H). Clusters preferentially located to 3′ UTRs and protein-coding regions (CDS) with differences between cell states (Figure 2D). Within 3′ UTRs and exons, the binding site distribution showed no specific localization preference (Figure S2I). The majority of non-3′ UTR clusters occurred on transcripts that were co-bound on the 3′ UTR (Figure S2J). Assessment of the overlap of IMP2-bound transcripts between HEK293T cells from an earlier study (Hafner et al., 2010) and our GBM spheroid and adherent cell cultures revealed numerous transcripts that were bound selectively in one or the other cell state or in HEK293T cells (Figure 2E). By integrating RNA-sequencing data of both spheroids and adherent cells, we found that IMP2 binding to transcripts was highly dependent on their cell-state-associated basal expression level, arguing against the possible influence of putative cell-state-dependent co-factors that may modulate IMP2 binding capability (Figure 2F; Figure S2K). Removal of genes that were differentially expressed in GSCs, their adherent progeny, and HEK293T cells markedly increased the proportion of transcripts bound in common (Figure S2L). Locally, 3′ UTR-binding sites in all three cell types shared a substantial overlap (25%–41%) in comparison to 10-fold randomization (2.7%–4.5%) and IMP1 (14%) or IMP3 (13%) (obtained from Hafner et al., 2010), with common sites having the highest mean coverage (Figure S2M). The post-transcriptional network controlled by IMP2 therefore varies significantly according to factors that determine mRNA expression levels, including the cellular context itself. At a local level, the RNA-binding sites display higher evolutionary conservation in both cell states compared to a randomized background and flanking regions (Figure S2N), and the 4-nt binding motif proposed by Hafner et al. was strongly over-represented in our cluster sequences (Figure S2O).

## IMP2 Binding Is Centered on Specific MicroRNA Recognition Elements, Including let-7 Target Sites

Next, we selected 3′ UTR-bound transcripts and analyzed the corresponding IMP2 binding specificity. We observed that IMP2 binds preferentially to 3′ UTRs with high A+T nucleotide content and MREs (Figure 3A; Figure S3A), both of which may constitute moderate predictors of IMP2 UTR binding using a general linear model with area under the curves (AUCs) of 0.77 and 0.75 in spheroid-forming and adherent cells, respectively (Figure S3B). Within 3′ UTRs, IMP2 bound directly to predicted MREs of a large number of transcripts, suggesting that it may contribute to miRNA-dependent transcript regulation. IMP2 binding to MREs was significantly higher than its binding to random and flanking regions in GSCs, adherent cells, and HEK293T cells (Figure 3B). Binding was particularly abundant to MREs corresponding to tumor suppressor miRNAs and miRNAs implicated in myogenesis, including miR-340, mir-143, miR-186, miR-202, and miR-1 (Figure S3C), with MRE binding coverage similar to that of let-7 targets (Figure S3D). Conversely, MREs of miRNAs involved in neurogenesis and brain development, including miR-9 (Figure S3D), miR-124, and miR-128, displayed no significant enrichment in IMP2 binding density. Together with a lack of correlation between miRNA expression and binding, this hints at a binding mechanism that does not implicate an obvious functional relationship with miRNAs (Figures S3E and S3C). For validated let-7 targets, such as *HMGA2*, we observed abundant IMP2 binding directly to specific MREs (Figure 3C).

Binding of IMP2 to MREs suggests a possible functional relationship with AGO2, the catalytic component of RISC. We therefore asked whether IMP2 and AGO2 reside in the same subcellular compartments. Transcript degradation and turnover occur in specific cellular compartments known as processing bodies (P-bodies) (Parker and Sheth, 2007), which contain most of the proteins involved in miRNA-mediated silencing, including AGO2 (Sen and Blau, 2005). Confocal microscopy of adherent GBM cells treated with antibodies against IMP2 and the P-body marker EDC4 (Yu et al., 2005) revealed co-localization of the two proteins, suggesting IMP2 interaction with RISC (Figure 3D). Co-localization of IMP2 and EDC4 was observed in both CD133$^+$ and CD133$^-$ sphere fractions, suggesting that IMP2 localization to P-bodies is not cell-state dependent (Figure S3F). Immunoprecipitation of IMP2 in RNase-free and RNase-treated lysates from spheroids followed by WB analysis revealed RNA-dependent association between AGO2 and IMP2 (Figure 3E), which was also observed in both CD133$^+$ and CD133$^-$ cells (Figure S3G).

## Modulation of IMP2 Levels Affects Target Gene Expression in Primary GBM

To address the global functional relevance of IMP2 binding to target transcripts and MREs, we conducted RNA sequencing on MGG4 and MGG8 tumor-derived cells that had been subjected to modulation of IMP2 expression. IMP2 was depleted by shRNA in spheroids and expressed in adherent cells at levels similar to those observed in native spheroids. Depletion of IMP2 in spheroids induced global downregulation of IMP2-bound compared to IMP2 unbound transcripts (Figure 3F). Conversely,

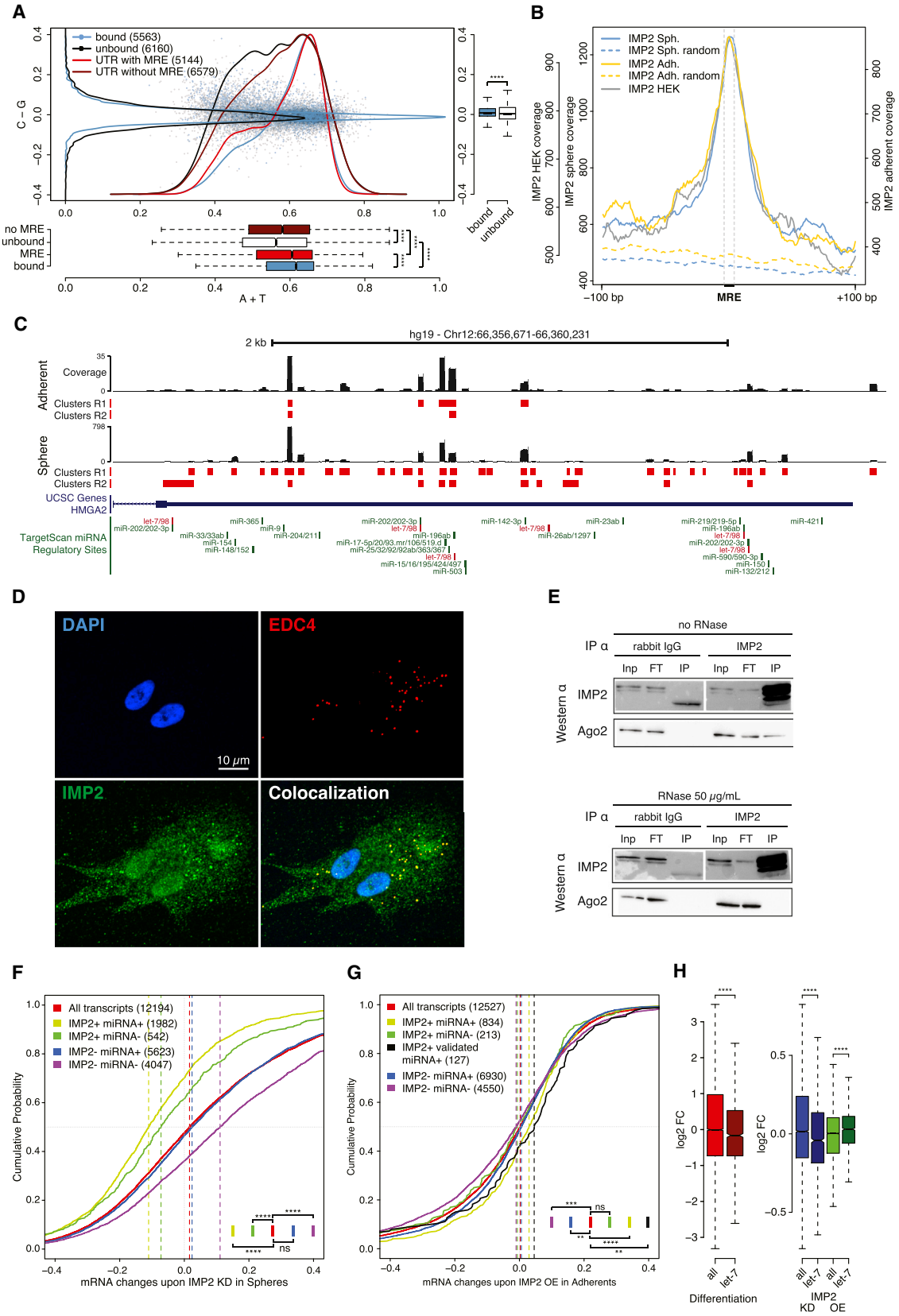


*(legend on next page)*

overexpression of IMP2 in adherent cells led to a general induction of bound transcripts, the most strongly induced being those bound by IMP2 on MREs located in previously validated miRNA targets (only targets of miRNAs expressed in GBM adherent cells were considered) (Figure 3G). Importantly, the same observations applied when restricting transcript selection to let-7 targets only (Figure 3H).

## IMP2 Modulates miRNA-Dependent Target Silencing of a Subset of let-7 Targets

Next, we explored the functional relevance of IMP2 binding to let-7 MREs. First, we confirmed that IMP2-bound let-7 targets identified by PAR-CLIP were significantly enriched in anti-IMP2 antibody RNA immunoprecipitates (RIPs) compared to isotype-matched antibody counterparts in all three primary cultures (Figure S4A) and that IMP2 depletion and overexpression affected both target mRNA and protein levels. qPCR analysis revealed that expression levels of the let-7 and IMP2-bound targets *HMGA1*, *HMGA2*, *IMP3*, and *CCND1* were lowered in spheroids depleted of IMP2 and increased in adherent cells overexpressing IMP2 (Figures 4A and 4C). Western blots of IMP3, CCND1 and HMGA2 confirmed these observations at the protein level (Figures 4B and 4D). Analysis of the same panel of targets by qPCR and WB using a different IMP2 shRNA yielded comparable results, rendering off-target effects unlikely (Figure S4B). To further verify the notion that IMP2 binding to MREs impairs miRNA-dependent target silencing, we performed RIP on AGO2 in IMP2-depleted and control spheroids (Figure 4E). Upon IMP2 depletion, loading of several targets onto AGO2 increased, supporting miRNA-RISC as the effector pathway for the observed changes in expression (Figure 4F). We then assessed the effect of let-7 axis blockade on spheres that were infected with a control vector or an shRNA targeting IMP2. Transfection of IMP2-depleted spheres with let-7 antagomiRs significantly rescued expression of the let-7 targets *IMP3*, *HMGA1*, *HMGA2*, and *CCND1* (Figure 4G; Figure S4C).

Finally, to validate the dependence of let-7-mediated target gene silencing on IMP2 binding to let-7 MREs, we stably transfected MGG8 adherent cells with reporter constructs composed of wild-type (WT) 3′ UTRs of *IMP3* and *HMGA2* ligated to sequences encoding firefly luciferase. After selection, IMP2 or an empty vector was stably introduced into these cells and luciferase activity was measured 72 hr later. Introduction of IMP2 increased luciferase activity of both *HMGA2* and *IMP3* reporter constructs compared to cells infected with the empty control vector (Figure 4H). Mutation of the unique let-7 site in the *IMP3* 3′ UTR and let-7 sites 2 and 3 (Figure 3C) in the *HMGA2* 3′ UTR abolished the increase in luciferase activity observed upon overexpression of IMP2 in cells expressing the WT 3′ UTR reporters (Figure 4H), suggesting that IMP2 exerts its protective functions primarily through prevention of let-7-mediated target gene silencing.

## Expression of LIN28B Rescues the Effects of IMP2 Depletion in GSCs

If IMP2 provides an alternative pathway for let-7 target protection with respect to LIN28B, then introduction of LIN28B into an IMP2-depleted background should rescue target transcript levels. To test this possibility, we depleted IMP2 by shRNA in MGG4 GSCs and 48 hr later expressed LIN28B using a lentiviral system, verifying both IMP2 depletion and LIN28B expression by WB (Figure 5A). LIN28B expression did not restore IMP2 (Figure 5A) but led to a robust decrease in mature let-7 levels, whereas depletion of IMP2 alone did not significantly alter mature let-7 expression (Figure 5B).

Expression levels of selected let-7 targets were then assessed by qPCR in spheroids depleted of IMP2, expressing LIN28B, or bearing a combination of LIN28B expression and IMP2 depletion, compared to spheres expressing control vectors. Introduction of LIN28B into spheres depleted of IMP2 restored *HMGA1*, *HMGA2*, *CCND1*, and *IMP3* expression (Figure 5C), whereas the predicted let-7 target transcript *BZW2*, which was unresponsive to IMP2 depletion, was also unresponsive to LIN28B expression.

A major effect of IMP2 depletion in GSCs was reduced clonogenicity, which was partially rescued by LIN28B expression

**Figure 3. Functional Relationship between IMP2 mRNA Binding and miRNAs**

(A) C−G and A+T content of IMP2 bound (blue) or non-bound (black) and MRE containing (red) or non-containing (dark red) 3′ UTRs in spheres. Each point represents a single 3′ UTR with densities of each group represented as lines and boxplots. The number of 3′ UTRs in each group is indicated in brackets. See also Figure S3A for adherent cells. Only non-overlapping 3′ UTRs longer than 50 bp and the top 5% of clusters are considered. Statistical significance was determined by Wilcoxon rank-sum test and is denoted as ****$p \leq 0.0001$.

(B) Sphere (blue), adherent (yellow), and HEK293T (gray; Hafner et al., 2010) cluster coverage in a 200-bp window centered on MREs with positive IMP2 binding. Matched 10× randomized samples (dashed line) indicate clusters randomized within cluster-containing 3′ UTRs. See Figure S3C for miRNA selection and S3D for let-7 and miR-9 MREs.

(C) UCSC genome browser view of the *HMGA2* 3′ UTR with TargetScan MRE predictions. The coverage of replicate 1 (R1) and clusters of both replicates (R1 and R2) are indicated. let-7 MREs are indicated in red.

(D) Immunofluorescence (IF) microscopy of IMP2 and EDC4 (P-body marker) expression in MGG8 adherent cells. Co-localization is shown in yellow (bottom right). Pearson's coefficient for co-localization is 0.602. See also Figure S3F for IF in spheres.

(E) Immunoprecipitation of endogenous IMP2 and rabbit control immunoglobulin G in RNase-free and RNase A-treated conditions followed by WB for IMP2 and AGO2; Inp, input; FT, unbound fraction; IP, bound fraction. See also Figure S3G for IP from lysates of spheres sorted for CD133 expression.

(F and G) Cumulative plot of log2 fold changes of gene expression in response to IMP2 depletion in spheres (F) and IMP2 overexpression in adherent cells (G). Gene subgroups are all transcripts (red); IMP2-bound transcripts that are targets (light green), experimentally validated targets (black, only G), and not targets (dark green) of expressed miRNAs; and IMP2 non-bound transcripts that are targets (blue) or not targets (violet) of expressed miRNAs. Statistical significance was determined by Kolmogorov-Smirnov test and is denoted as ****$p \leq 0.0001$, ***$p \leq 0.001$, **$p \leq 0.01$, and ns (non-significant).

(H) Distribution of log2 fold changes in expression of all genes and let-7 target genes between spheres and adherent cells (left), IMP2 depletion (knockdown [KD]) in spheres (right) and IMP2 overexpression (OE) in adherent cells (right). Statistical significance was determined by Wilcoxon rank-sum test and is denoted as ****$p \leq 0.0001$.

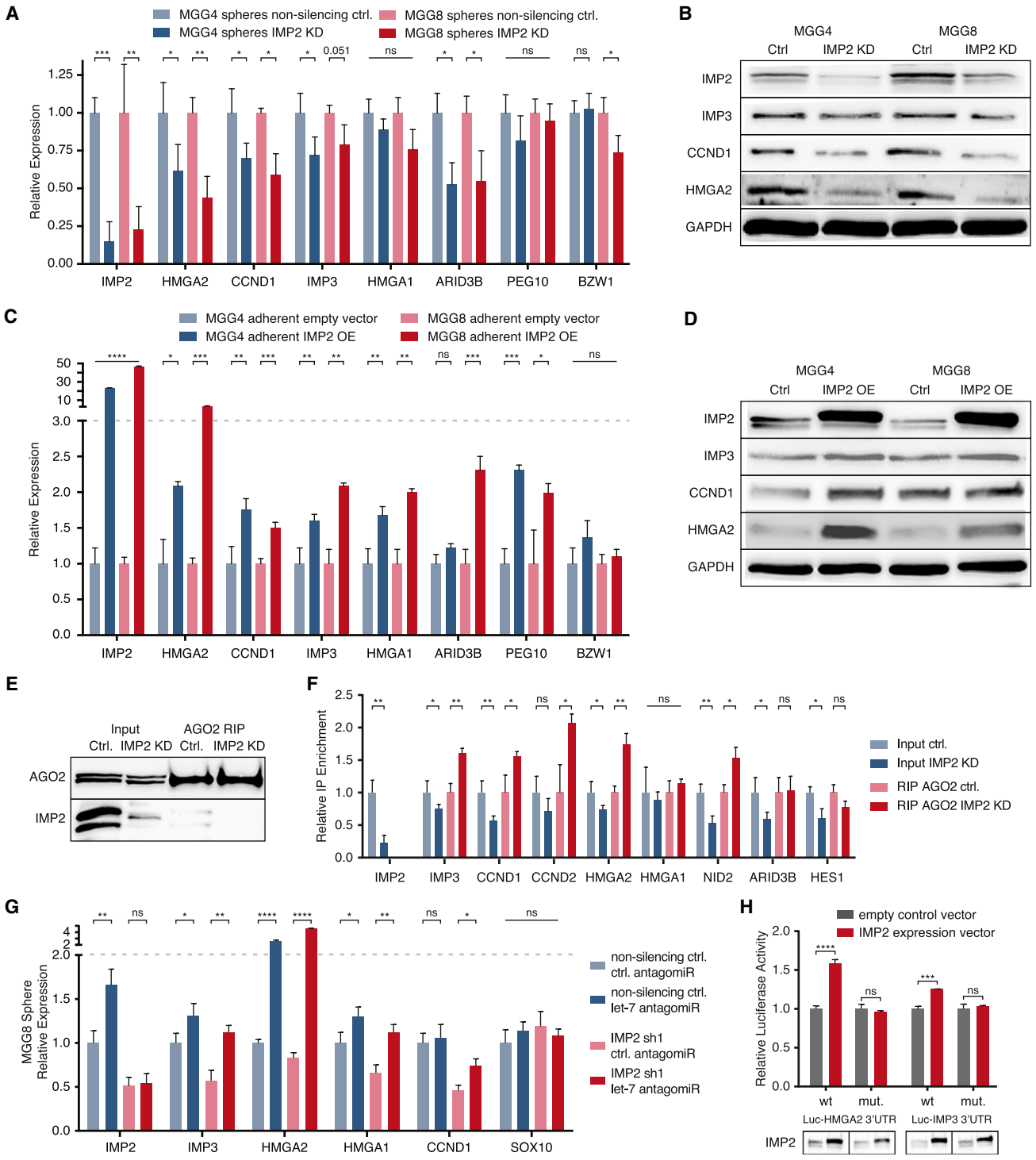


**Figure 4. Effects of IMP2 Modulation on let-7 Target Gene Expression**

(A) Relative expression of predicted IMP2-bound let-7 target genes upon IMP2 depletion in MGG4 and MGG8 GSCs as assessed by qPCR. Data are presented as the mean ± SEM of three experiments. p values are denoted as **p ≤ 0.01, *p ≤ 0.05, and ns (non-significant). See also Figure S4B for an alternative shRNA targeting IMP2.

(B) WB of IMP2, IMP3, CCND1, and HMGA2 in MGG4 and MGG8 GSCs depleted (KD) or not of IMP2 using GAPDH as a loading control. See also Figure S4B for an alternative shRNA targeting IMP2.

(C) Relative expression of predicted IMP-2-bound let-7 target genes upon overexpression (OE) of IMP2 in MGG4 and MGG8 adherent cells as assessed by qPCR. The mean ≥ SEM of three experiments is shown. p values are denoted as ****p ≤ 0.0001, ***p ≤ 0.001, **p ≤ 0.01, *p ≤ 0.05, and ns (non-significant).

*(legend continued on next page)*

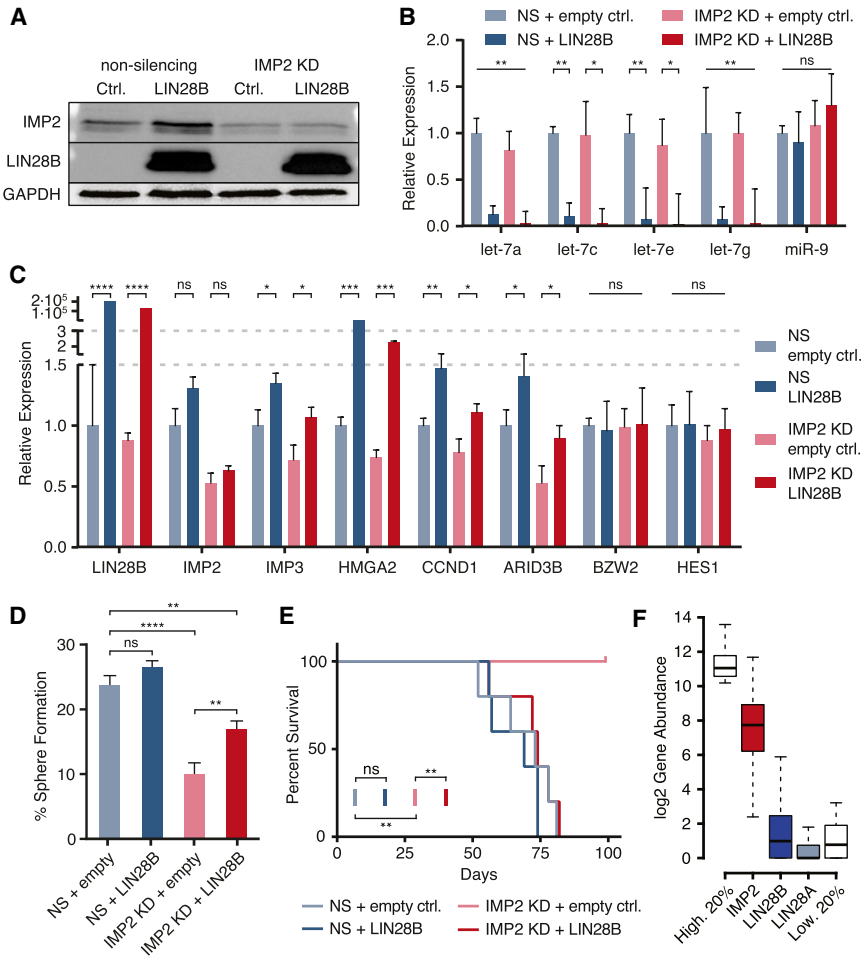


**Figure 5. LIN28B-Mediated Rescue of the Effects of IMP2 Depletion on GSC Clonogenicity and Tumor Initiation**

(A) WB of IMP2 and LIN28B in MGG4 spheroids under control (left) or IMP2 KD (right) conditions, each transfected with an empty vector or expressing LIN28B. GAPDH provided a loading control.

(B) Relative expression of mature let-7 family members in MGG4 GSCs upon depletion of IMP2 alone or in combination with LIN28B expression, normalized to non-silencing (NS) and empty vector conditions. miR-9, whose maturation is LIN28 independent, is provided as a control. Data are presented as the mean ± SEM of two experiments. p values are denoted as $^{**}p \leq 0.01$, $^{*}p \leq 0.05$, and ns (non-significant).

(C) Relative expression of putative let-7 target genes in response to IMP2 depletion, LIN28B expression, or a combination of both normalized to non-silencing (NS) and empty vector controls in MGG4 GSCs. *HES1* is a validated miR-9 target not bound by IMP2 in GSCs used as a control. Data are presented as the mean ± SEM of two experiments. p values are denoted as $^{****}p \leq 0.0001$, $^{***}p \leq 0.001$, $^{**}p \leq 0.01$, $^{*}p \leq 0.05$, and ns (non-significant).

(D) Clonogenic assay of MGG4 GSCs bearing control vectors (empty and non-silencing, NS, vectors), LIN28B expression, IMP2 KD and a combination of LIN28B expression and IMP2 KD. The mean ± SEM of three independent experiments is shown. ns, non-significant, $^{**}p \leq 0.01$, and $^{****}p \leq 0.0001$.

(E) Survival curve of mice injected with 10,000 MGG4 GSCs expressing control vectors, LIN28B, IMP2 shRNA (KD) or a combination of LIN28B and IMP2 KD. Statistical significance was calculated using log-rank test and is denoted as $^{**}p \leq 0.01$ and ns (non-significant) (five mice per group).

(F) Log2 expression levels of IMP2 and LIN28A/B according to the 166 TCGA HiSeq v2 GBM dataset. The 20% highest and lowest expressed genes are included for comparison.

(Figure 5D). To extend our observations in vivo, we injected five mice each orthotopically with 10,000 MGG4 spheres expressing control non-silencing vectors, depleted of IMP2, expressing LIN28, or bearing a combination of IMP2 depletion and LIN28B expression. Between 56 and 81 days following injection, all mice that had received cells expressing control vectors, LIN28B, and LIN28B combined with IMP2 depletion succumbed to tumors, whereas mice bearing cells depleted of IMP2 alone manifested no signs of tumor growth (Figure 5E). All of the tumors displayed typical GBM histology with robust angiogenesis, extensive necrosis, and a high degree of invasiveness (data not shown). Importantly, the rate of tumor development from control, LIN28B-expressing, and IMP2-depleted/LIN28B-rescued cells was comparable.

TCGA database interrogation of primary GBM tumor bulk samples indicates that the expression of both *LIN28A* and

(D) WB of IMP2, IMP3, CCND1, and HMGA2 in MGG4 and MGG8 adherent cells overexpressing IMP2 or containing empty vector using GAPDH as a loading control.

(E) WB of input and 10% AGO2 RIP in control and IMP2 KD conditions in MGG4 GSCs as a control for the immunoprecipitated quantity.

(F) Transcript levels in control and IMP2 KD cells in input and AGO2 RIP fractions. Levels of input in IMP2 KD and AGO2 RIP fractions are normalized to the respective non-silencing control. p values are denoted as $^{**}p \leq 0.01$, $^{*}p \leq 0.05$, and ns (non-significant).

(G) Relative expression of predicted IMP2-bound let-7 targets upon IMP2 depletion and/or treatment with let-7 antagomiRs as assessed by qPCR in MGG8 cells. SOX10, which is not a let-7 target but is IMP2 bound, is used as a control. Bars represent the mean ± SD. See also Figure S4C for the same experiment on MGG4 cells. p values are denoted as $^{**}p \leq 0.01$, $^{*}p \leq 0.05$, and ns (non-significant).

(H) Reporter assays for wild-type (wt) and let-7 binding site mutated (mut.) *HMGA2* and *IMP3* 3′ UTRs performed in MGG8 adherent cells stably transfected with luciferase reporter vectors and expressing either an empty vector or IMP2. Luciferase activity was normalized to total protein content and transfection with empty vector. Bars represent mean ± SD. ns, non-significant, $^{***}p \leq 0.001$, and $^{****}p \leq 0.0001$.

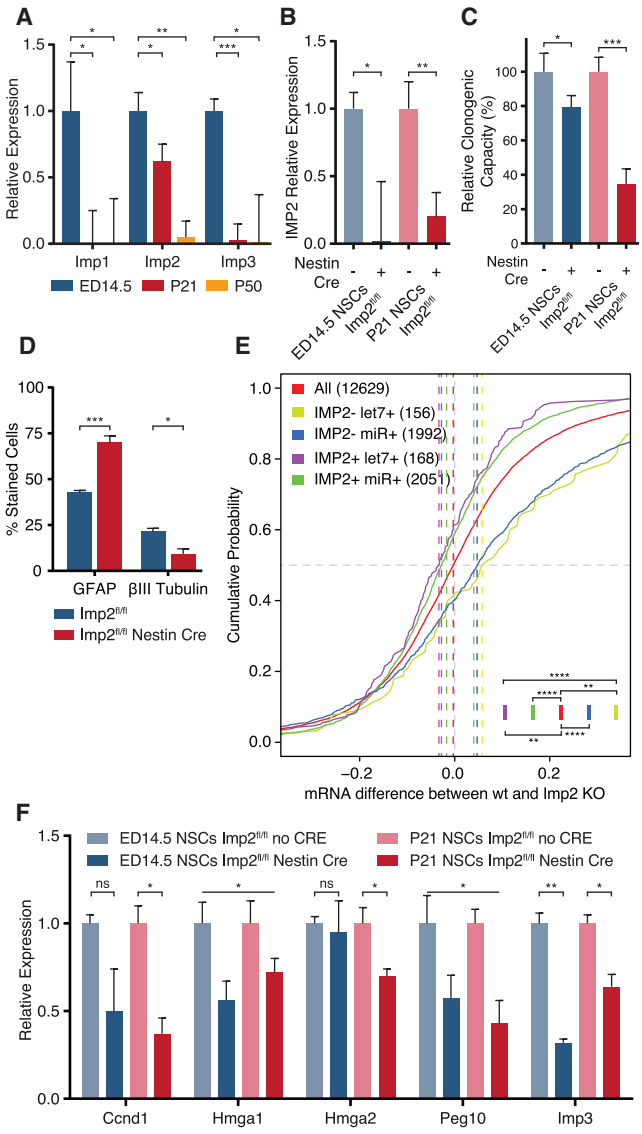


**Figure 6. IMP2 in Neural Stem Cells**

(A) Relative expression of *IMP2* in mouse embryo (E14.5 [ED14.5]) and P21 and P50 brains as assessed by qPCR normalized to E14.5. Data are presented as the mean ± SEM of three experiments. p values are denoted as ***p ≤ 0.001, **p ≤ 0.01, and *p ≤ 0.05.

(B) Relative expression of *IMP2* in NSC conditional *Imp2* KO animals (*Imp2*$^{fl/fl}$ × Nestin Cre) as assessed by qPCR, normalized to WT animals (*Imp2*$^{fl/fl}$). Data are presented as the mean ± SEM of two experiments. p values are denoted as **p ≤ 0.01 and *p ≤ 0.05.

(C) Clonogenic assay of WT and *Imp2* KO NSCs derived from E14.5 and P21 mouse brains, normalized to WT cells. Data are presented as the mean ± SEM of three independent experiments. ***p ≤ 0.001 and *p ≤ 0.05.

(D) Percentage of positive cells for GFAP (astrocytic marker) and BIII-tubulin (neuronal marker) as assessed by immunofluorescence microscopy. Bars represent the mean ± SD. p values are denoted as ***p ≤ 0.001 and *p ≤ 0.05.

(E) Cumulative plot of log2 fold changes of gene expression in response to *Imp2* knockout in E14.5 and P21 brains. Gene subgroups are all transcripts (red), transcripts with no IMP2 binding in human and mouse let-7 targets (light green), no IMP2 binding in human and targets of any miRNA (blue), IMP2 binding in human and mouse let-7 targets (violet), and IMP2 binding in human and targets of any miRNA (green). Statistical significance was determined by Kolmogorov-Smirnov test and is denoted as ****p ≤ 0.0001 and **p ≤ 0.01.

(F) Relative expression of putative IMP2-bound validated let-7 target genes upon depletion of IMP2 in NSCs as assessed by qPCR normalized to WT. Data are presented as the mean ± SEM of two experiments. p values are denoted as **p ≤ 0.01, *p ≤ 0.05, and ns (non-significant).

*LIN28B* is marginal compared to *IMP2* (Figure 5F). Although we cannot formally exclude the possibility that a small fraction of cells display higher expression of *LIN28A/B*, these observations argue against significant expression of LIN28 in primary GBM tumors, consistent with the status of the primary cells used in this study.

## IMP2 Expression in Neural Stem Cells

IMP2 is highly expressed in the developing brain with a peak around mid-gestation in mice (Nielsen et al., 1999) and its depletion in NSCs favors astrocytic lineage commitment (Fujii et al., 2013). Normal stem cells share some of their properties with CSCs and are believed to be candidate cells of origin of various malignancies (Visvader, 2011). We therefore addressed possible similarities between GSCs and NSCs with respect to IMP2-dependent control of let-7 target gene silencing.

We examined *Imp2* expression in brains extracted from *Imp2* floxed (*Imp2*$^{fl/fl}$) embryos and mice at different stages of development (embryonic day 14.5 [E14.5], postnatal day 21 [P21], and P50). Consistent with previous work, *Imp2* expression was highest during embryonic development (Nielsen et al., 1999; Nishino et al., 2013), with a gradual decrease following birth (Figure 6A). Immunohistochemical staining of brain sections revealed strong IMP2 expression at E14.5, detectable expression at P21, and marginal expression at P50 (data not shown). To delete *Imp2* in NSCs, we crossed *Imp2*$^{fl/fl}$ mice with a strain expressing Cre recombinase under the control of the nestin promoter (Dubois et al., 2006). We then derived NSCs from *Imp2*$^{fl/fl}$ mice (WT) and *Imp2*$^{fl/fl}$ Nestin Cre animals (knockout [KO]) of E14.5 and P21 for further analysis. qPCR analysis confirmed *Imp2* suppression in KO-mice-derived NSCs compared to controls (Figure 6B). Similar to its effect in GSCs, *Imp2* depletion impaired NSC clonogenicity, and more strongly so in P21 mice, when *Imp1* and *Imp3* are no longer expressed (Figures 6A and 6C).

Let-7 and its targets are key regulators of NSC maintenance and differentiation (Nishino et al., 2008; Yu et al., 2015) and, along with let-7 target sites, are highly conserved during evolution and across species (Pasquinelli et al., 2000). In addition to their actions during development, let-7 family members are required for differentiation of glial progenitor cells to astrocytes (Shenoy et al., 2015). Consistent with previous reports using shRNAs targeting *Imp2* in NSCs, *Imp2* KO NSCs displayed increased astrocytic and reduced neuronal differentiation (Figure 6D). Whether this phenotype is the result of modulation of the let-7 axis, which is itself involved in the control of differentiation of neural progenitor cells, remains to be addressed. To determine whether IMP2 has a similarly conserved role toward let-7 target transcripts in NSCs, we sequenced NSC RNA (after 7 days of NSC culture in vitro) derived from WT and KO E14.5 embryos and P21 mice. We made the assumption that

IMP2-bound transcripts are conserved between GSCs and NSCs and analyzed the effect of IMP2 depletion on putatively bound transcripts in NSCs. Consistent with our observations in GSCs, let-7 target transcript levels were lower in *Imp2* KO NSCs than in controls, supporting a protective role for IMP2 (Figure 6E). Validation by qPCR of the RNA-sequencing data for the let-7 targets *Ccnd1*, *Peg10*, *Hmga1*, *Hmga2*, and *Imp3* confirmed these results (Figure 6F).

## DISCUSSION

Comparison of miRNA expression profiles of GSCs and their non-tumorigenic progeny from three independent primary GBMs revealed differential expression of a subset of miRNAs between the two cell states but comparable and elevated expression of mature tumor and stemness suppressive let-7 family members. Consistent with these findings, the let-7 maturation repressors LIN28A and LIN28B, which are re-expressed in ~15% of predominantly undifferentiated malignant tumors as well as in CSCs of diverse cancer types (Nguyen et al., 2014; Viswanathan et al., 2009), were undetectable. Expression of let-7 target genes in GSCs in the face of intact let-7 maturation therefore argued for an alternative mechanism that impairs the ability of let-7 family members to induce target gene silencing. Prevention of miRNA-mediated gene silencing by RBPs that bind to or in close proximity to MREs on target mRNAs provided a readily testable alternative. An elegant study reported this to be the mechanism whereby the RBP PTB, a target of miR-124, can protect its bound transcripts, including its own, from the action of miR-124 (Xue et al., 2013). We previously showed that the RBP IMP2, which contains two let-7 MREs in its 3′ UTR, is highly expressed in GSCs and essential for their maintenance and tumor initiating capacity (Janiszewska et al., 2012). Co-expression of IMP2 and several validated let-7 targets in GSCs, as revealed by TCGA expression analysis, supports a functional relationship between IMP2 and let-7 analogous to that between PTB and miR-124, which our observations strongly favor.

PAR-CLIP, applied to a primary proneural GBM grown as a GSC-enriched spheroid culture and its non-tumorigenic adherent progeny, identified the mRNA repertoire bound to IMP2 on a transcriptome-wide scale. Analysis of IMP2 binding to mRNA revealed that IMP2 preferentially localizes to 3′ UTRs with high AT content and MREs and, more importantly, showed that its binding density is enriched on a subset of MREs, including let-7 target sites, suggesting that IMP2 protects these transcripts from miRNA-mediated silencing. Consistent with this notion, we found that transcripts bound by IMP2 on MREs of previously validated miRNA targets constitute the most strongly suppressed class of mRNAs upon IMP2 depletion. Thus, protection from RISC/AGO-mediated silencing by IMP2 explains the observed expression of both let-7 family miRNAs and their target genes. Accordingly, depletion of IMP2 led to decreased expression of the let-7 target gene repertoire, which includes genes implicated in oncogenesis and maintenance of stemness. As IMP2 is highly expressed in all GBM molecular subtypes, its functional role is most likely similar irrespective of subclass.

IMP2 protection is not limited to let-7 target genes. Consistent with this notion, PAR-CLIP revealed increased binding density of IMP2 on MREs targeted by miRNAs that were not expressed in GBM. Although let-7 target genes displayed the highest fold changes in response to IMP2 depletion and overexpression, IMP2-bound targets of other expressed miRNAs responded in a similar fashion. Ultimately, the effect of IMP2 on target transcripts most likely varies according to the cell-context-dependent repertoire of mRNAs, miRNAs, and RBPs.

Comparison of our data to previously published PAR-CLIP studies of IMP1-3 in HEK293T cells revealed strong overlap of their binding sites, including let-7 MREs. Furthermore, a recent study suggested that IMP3 is co-expressed with HMGA2 in a broad range of solid tumors and revealed that IMP3 has the ability to safeguard the *HMGA2* transcript from let-7 degradation (Jønson et al., 2014), suggesting functional redundancy between IMP2 and IMP3 for at least a subset of transcripts. To what degree IMP3 may participate in IMP2-dependent protection of let-7 target genes in GSCs remains to be determined. However, it is conceivable that IMP3 expression provides a fail-safe mechanism to ensure preservation of key let-7 target genes required for GSC maintenance. Unlike IMP3, IMP2 co-localized with P-bodies and co-immunoprecipitated with AGO2 in an RNA-dependent fashion, suggesting that IMP2 and AGO2 are not located in separate cellular compartments, as IMP3 and AGO2 appear to be (Jønson et al., 2014). Thus, despite putative partial functional redundancy, IMP2 and IMP3 may employ distinct effector pathways.

Suppression of let-7 target gene expression upon IMP2 depletion was accompanied by loss of GSC clonogenicity and tumor initiating capacity. Overexpression of IMP2, on the other hand, did not alter the GSC phenotype, suggesting that the maximal effect of IMP2 on clonogenicity and tumor initiation had been reached within the physiological expression level in GSCs. The ability of LIN28B to rescue the IMP2 depletion phenotype without restoring IMP2 expression reflects the distinct mechanisms that LIN28 and IMP2 employ to maintain let-7 target gene expression. The high selectivity of LIN28 for inhibition of let-7 biogenesis argues that the observed phenotypic rescue is primarily due to restoration of let-7 and not some unrelated miRNA target gene expression. However, the participation of putative let-7-independent mechanisms cannot be formally excluded. In addition to regulating let-7 target gene expression, albeit by different mechanisms, IMP2 and LIN28 share a broad range of intriguing functional similarities. They include a temporally and spatially overlapping expression pattern during normal development (Balzer et al., 2010; Christiansen et al., 2009), the ability to enhance translation of IGF-2 (Polesskaya et al., 2007; Dai et al., 2011), behavior as bona fide let-7 targets, the ability to block glial differentiation (Fujii et al., 2013; Balzer et al., 2010), and implication in cellular bioenergetics. LIN28 is implicated in the regulation of glucose metabolism (Zhu et al., 2011) and in coordinating growth through let-7-dependent regulation of numerous metabolic genes. (Zhu et al., 2011; Shyh-Chang and Daley, 2013). LIN28 can also enhance oxidative phosphorylation (OXPHOS) during wound healing through let-7-independent mechanisms, and inhibition of OXPHOS reduces its ability to promote tissue repair (Shyh-Chang et al., 2013). Similarly, IMP2 regulates metabolism by promoting OXPHOS in GSCs, in part through physical interactions with mitochondria

(Janiszewska et al., 2012). Whether or not let-7 blockade is implicated in this particular function of IMP2 remains to be determined, but regulation of GSC bioenergetics may constitute a mechanism that contributes to both IMP2 and LIN28-mediated CSC maintenance.

IMP2 implication in GSC maintenance reflects its physiological role in NSC development. In NSCs, IMP2 is expressed well after IMP1 and IMP3 repression has occurred and protects let-7 target transcripts, reminiscent of the situation in GSCs. IMP2 depletion in NSCs led to global downregulation of putatively bound let-7 targets, which were similarly repressed in IMP2-depleted GSCs, and reduced clonogenicity, indicating conserved function between normally developing cells and GSCs.

Taken together, we have shown that the RBP IMP2 protects let-7 miRNA family target genes from silencing and promotes GSC clonogenicity and tumor-initiating capacity. As such, it provides an important alternative mechanism for CSC maintenance to LIN28-dependent inhibition of let-7 biogenesis. Therapeutic targeting of IMP2-dependent let-7 target gene protection may provide an attractive option toward abolishing cellular hierarchy in GBM, which, if effective, could lead to major improvement in the prognosis of one of the deadliest human malignancies.

## EXPERIMENTAL PROCEDURES

### Cell Culture

GSCs used were characterized in previous studies (Wakimoto et al., 2012; Rheinbay et al., 2013; Suvà et al., 2014). GSCs were grown in Neurobasal medium (Invitrogen) supplemented with L-glutamine (GIBCO), B27, N2 (Invitrogen), and recombinant hEGF and hFGF2 (R&D Systems). GSCs differentiation was induced by adding 10% fetal calf serum (FCS) and removing growth factors for 7 days on plates coated with 100 μg/ml poly-D-lysine and 15 μg/ml laminin (Sigma-Aldrich). For further details, see Supplemental Experimental Procedures.

### Clonogenic Assays

GSCs infected with non-silencing or IMP2 pGIPZ shRNA (RHS4346 and V3LHS-393362, Dharmacon) were mechanically dissociated and plated at single-cell density in 96-well low-adherence plates. Sphere numbers were assessed after 2 weeks by imaging and statistical significance was determined with Student's t test using GraphPad Prism 6 software.

### Lentiviral Infections and Transfections

Lentiviruses produced in HEK293T transfected with the plasmid of interest, GAG/POL, and VSV using FuGene HD (Promega) were used to infect GBM cells. Cells were infected for 16 hr and selected in 2 μg/ml puromycin for 4 days. V3LHS-393362 for IMP2 depletion (IMP2 sh-1) and a scrambled shRNA (Dharmacon) were used. The targeting sequence and vector corresponding to IMP2 sh-2 were described previously (Janiszewska et al., 2012). For let-7 miRNA blockade, pooled scrambled or let-7 antagomiRs (Exiqon) were transfected into GBM cells with RNAiMAX (Thermo Fischer Scientific) and the cells were harvested 48 hr later. For further details, see the Supplemental Experimental Procedures.

### RNA Extraction, cDNA Synthesis, and qPCR

RNA was extracted using miRCURY (Exiqon) with DNase treatment (QIAGEN). 500 ng RNA was reverse transcribed using M-MLV (Promega). qPCR was performed with TaqMan Universal PCR (Applied Biosystems) or Power SYBR green (Applied Biosystems). Each qPCR reaction was performed in triplicate and normalized to PPIA and 18S (Thermo Fisher Scientific). For miRNA-qRT-PCR, 50 ng template RNA was reverse transcribed with a universal cDNA synthesis kit (Exiqon). qPCR was done in triplicate with primers for mature miRNAs (microRNA LNA PCR primer sets, Exiqon) normalized to RNU5G and SNORD49a (Exiqon). Statistical significance was determined using Student's t test. For further details and primers used, see the Supplemental Experimental Procedures.

### PAR-CLIP

PAR-CLIP was performed according to Hafner et al. (2010), with minor modifications. For GSC-enriched spheroids, $\sim 10^8$ dissociated cells were incubated overnight with 100 μM 4SU (Sigma-Aldrich) and crosslinked with 0.36 J/cm$^2$ total 365-nm irradiation. For adherent GBM cells, $\sim 3 \times 10^8$ subconfluent cells were crosslinked with 0.15 J/cm$^2$ total 365-nm irradiation. Before clearing, both cell lysates were treated with RNase T1 and RNase-free DNase I (Fermentas) and sonicated. Immunoprecipitation was performed with 20 μg anti-IMP2 (MBL) antibody for 3 hr. For further details and antibodies used, see the Supplemental Experimental Procedures.

### Sequence Alignment and Computational Analysis

Sequenced PAR-CLIP reads were adaptor-trimmed with a custom script and aligned to the hg19 human genome using Bowtie 0.12.9 (Langmead et al., 2009). Cluster identification was done with wavClusteR 2.2.0 (Comoglio et al., 2015). RNA-sequencing reads were aligned to the hg19 human genome build using TopHat 2.0.12 (Trapnell et al., 2009). Differential expression analysis was done in R 3.2.0 using edgeR 3.10.2 (Robinson et al., 2010). Further analysis was performed with custom scripts based on Bioconductor functions (Huber et al., 2015), and the results are available upon request. See also the Supplemental Experimental Procedures.

### RNA Immunoprecipitation, Co-immunoprecipitation of IMP2, and Western Blots

RIP assay kit for microRNA (MBL International) was used according to the manufacturer's recommendations. 5% input and 40 μg protein lysates from $2 \times 10^7$ cells were used for RNA extraction and WB, respectively. Immunoprecipitation with anti-AGO2 and isotype-matched antibodies was performed with 5 mg pre-cleared lysates at 4°C for 2 hr. 10% of final beads were used for WB and 90% for RNA extraction. 100 ng input and RIP RNA was reverse transcribed and analyzed by qPCR. Enrichment of targets was calculated using ddCT (Livak and Schmittgen, 2001). For further details and antibodies used, see the Supplemental Experimental Procedures.

### Immunofluorescence

Immunofluorescence (IF) was performed as described previously (Janiszewska et al., 2012) using a Leica SP5AOBS confocal microscope at the Imaging Core Facility of the University of Lausanne. Co-localization was calculated using ImageJ (ImageJ, Rasband, W.S., NIH). For additional details, see the Supplemental Experimental Procedures.

### Neural Stem Cell Extraction and Culture

Extraction of NSCs from mouse brains was performed as described previously (Azari et al., 2010, 2011). NSCs were cultured in NeuroCult NSC Basal Medium with 10% NeuroCult Proliferation Supplement (STEMCELL Technologies) and 20 ng/ml EGF. For post-natal-derived NSCs, 10 ng/ml FGF2 and 2 μg/ml heparin were added. Neurospheres were grown for 6–8 days in ultra-low-adherence flasks (Corning Life Sciences) and passaged every 4–7 days using Accutase (STEMCELL Technologies). Differentiation capacity was assessed by adding 10% NeuroCult Differentiation Supplement (STEMCELL Technologies) to the medium for 10 days followed by IF analysis using anti-GFAP (astrocytic) and anti-Tuj-1 (neuronal) antibodies.

### Mouse Strains and Genotyping

*Imp2* floxed mice were a gift of Prof. Bernard Thorens (University of Lausanne) produced by Genoway (C57BL6 background). CNS knockouts were generated by breeding *Imp2* floxed with Nestin-cre mice (C57BL6 background) obtained from the Transgenic Core Facility of Ecole Polytechnique Fédéral de Lausanne. The recombination profile has been described previously (Dubois et al., 2006). Experiments were performed under license number VD2488 (approved by the Service de la Consommation et des Affaires Vétérinaires, Epalinges, Switzerland). All mice were genotyped and knockout efficiencies tested. See also Supplemental Experimental Procedures.

### miRNA Array

Probe intensities provided by the facility were analyzed using limma. Log-transformed values were normalized between arrays using cyclic-loess. For hierarchical clustering, the 20 miRNAs with highest fold changes were clustered by complete linkage using base R (3.2.0) functions.

### Luciferase Assays and 3′ UTR Site-Directed Mutagenesis

The 3′ UTRs of *HMGA2* and *IMP3* were cloned into a lentiviral reporter vector (Lenti-reporter-Luc Vector, ABMgood). Cytosine bases in let-7 MREs were mutated to guanine using a QuickChange II XL site-directed mutagenesis kit (Agilent Technologies) according to the manufacturer's recommendations. MGG adherent cells were infected with reporter vectors and selected with puromycin. 72 hr after IMP2 or control transfection, samples were processed with a luciferase assay system (Promega) and measured on a SynergyMX instrument (BioTek Instruments). Luciferase activity was normalized to total protein content and statistical significance calculated using Student's t test with GraphPad Prism 6 software.

### Xenografts of Glioma Stem Cells

Intracranial xenografts were performed as previously described (Suvà et al., 2014). Experiments were performed under license number VD2852 (approved by the Service de la Consommation et des Affaires Vétérinaires, Epalinges, Switzerland). Statistical significance was determined using log-rank test with GraphPad Prism 6 software.

## ACCESSION NUMBERS

The accession number for the microarray and deep-sequencing data reported in this paper is GEO: GSE73847.

## SUPPLEMENTAL INFORMATION

Supplemental Information includes Supplemental Experimental Procedures, four figures, and two tables and can be found with this article online at http://dx.doi.org/10.1016/j.celrep.2016.04.086.

## AUTHOR CONTRIBUTIONS

N.D. and T.S designed and performed the experiments, and T.B.S. did bioinformatics analysis. N.D., T.B.S., and I.S. wrote the manuscript. P.M. and A.C. helped with various experiments and mouse work. P.P. helped with bioinformatics. M.J., N.R., and M.-L.S. helped with experimental design and data analysis. R.P. supervised PAR-CLIP experiments. I.S. designed and supervised experiments and wrote the manuscript.

## ACKNOWLEDGMENTS

We thank Jean-Christophe Stehle of the mouse pathology facility for xenograft processing, Prof. Bernard Thorens for sharing IMP2 floxed mouse strain, and the animal facility team of Epalinges. This work was supported by the Swiss National Scientific Foundation (grant 310030-150024), the Swiss Cancer League (grant KLS-3365-02-2014), and a MEDIC Foundation grant to I.S. N.D. was supported by the Swiss National Scientific Foundation MD-PhD program (grant 323630_145251).

Received: November 6, 2015
Revised: February 19, 2016
Accepted: March 24, 2016
Published: May 12, 2016

## REFERENCES

Azari, H., Rahman, M., Sharififar, S., and Reynolds, B.A. (2010). Isolation and expansion of the adult mouse neural stem cells using the neurosphere assay. J. Vis. Exp. *8–11*, 2393.

Azari, H., Sharififar, S., Rahman, M., Ansari, S., and Reynolds, B.A. (2011). Establishing embryonic mouse neural stem cell culture using the neurosphere assay. J. Vis. Exp. *1–4*, 2457.

Balzer, E., Heine, C., Jiang, Q., Lee, V.M., and Moss, E.G. (2010). LIN28 alters cell fate succession and acts independently of the let-7 microRNA during neurogliogenesis in vitro. Development *137*, 891–900.

Bao, S., Wu, Q., McLendon, R.E., Hao, Y., Shi, Q., Hjelmeland, A.B., Dewhirst, M.W., Bigner, D.D., and Rich, J.N. (2006). Glioma stem cells promote radioresistance by preferential activation of the DNA damage response. Nature *444*, 756–760.

Bartel, D.P. (2009). MicroRNAs: target recognition and regulatory functions. Cell *136*, 215–233.

Bell, J.L., Wächter, K., Mühleck, B., Pazaitis, N., Köhn, M., Lederer, M., and Hüttelmaier, S. (2013). Insulin-like growth factor 2 mRNA-binding proteins (IGF2BPs): post-transcriptional drivers of cancer progression? Cell. Mol. Life Sci. *70*, 2657–2675.

Boyerinas, B., Park, S.M., Shomron, N., Hedegaard, M.M., Vinther, J., Andersen, J.S., Feig, C., Xu, J., Burge, C.B., and Peter, M.E. (2008). Identification of let-7-regulated oncofetal genes. Cancer Res. *68*, 2587–2591.

Chen, J., Li, Y., Yu, T.-S., McKay, R.M., Burns, D.K., Kernie, S.G., and Parada, L.F. (2012). A restricted cell population propagates glioblastoma growth after chemotherapy. Nature *488*, 522–526.

Christiansen, J., Kolte, A.M., Hansen, Tv., and Nielsen, F.C. (2009). IGF2 mRNA-binding protein 2: biological function and putative role in type 2 diabetes. J. Mol. Endocrinol. *43*, 187–195.

Comoglio, F., Sievers, C., and Paro, R. (2015). Sensitive and highly resolved identification of RNA-protein interaction sites in PAR-CLIP data. BMC Bioinformatics *16*, 32.

Dai, N., Rapley, J., Angel, M., Yanik, M.F., Blower, M.D., and Avruch, J. (2011). mTOR phosphorylates IMP2 to promote IGF2 mRNA translation by internal ribosomal entry. Genes Dev. *25*, 1159–1172.

De Vito, C., Riggi, N., Cornaz, S., Suvà, M.L., Baumer, K., Provero, P., and Stamenkovic, I. (2012). A TARBP2-dependent miRNA expression profile underlies cancer stem cell properties and provides candidate therapeutic reagents in Ewing sarcoma. Cancer Cell *21*, 807–821.

Dubois, N.C., Hofmann, D., Kaloulis, K., Bishop, J.M., and Trumpp, A. (2006). Nestin-Cre transgenic mouse line Nes-Cre1 mediates highly efficient Cre/loxP mediated recombination in the nervous system, kidney, and somite-derived tissues. Genesis *44*, 355–360.

Fujii, Y., Kishi, Y., and Gotoh, Y. (2013). IMP2 regulates differentiation potentials of mouse neocortical neural precursor cells. Genes Cells *18*, 79–89. http://dx.doi.org/10.1111/gtc.12024.

Gerstberger, S., Hafner, M., and Tuschl, T. (2014). A census of human RNA-binding proteins. Nat. Rev. Genet. *15*, 829–845.

Goswami, S., Tarapore, R.S., Poenitzsch Strong, A.M., TeSlaa, J.J., Grinblat, Y., Setaluri, V., and Spiegelman, V.S. (2015). MicroRNA-340-mediated degradation of microphthalmia-associated transcription factor (MITF) mRNA is inhibited by coding region determinant-binding protein (CRD-BP). J. Biol. Chem. *290*, 384–395.

Hafner, M., Landthaler, M., Burger, L., Khorshid, M., Hausser, J., Berninger, P., Rothballer, A., Ascano, M., Jr., Jungkamp, A.-C., Munschauer, M., et al. (2010). Transcriptome-wide identification of RNA-binding protein and microRNA target sites by PAR-CLIP. Cell *141*, 129–141.

He, L., and Hannon, G.J. (2004). MicroRNAs: small RNAs with a big role in gene regulation. Nat. Rev. Genet. *5*, 522–531.

Heo, I., Joo, C., Kim, Y.K., Ha, M., Yoon, M.J., Cho, J., Yeom, K.H., Han, J., and Kim, V.N. (2009). TUT4 in concert with Lin28 suppresses microRNA biogenesis through pre-microRNA uridylation. Cell *138*, 696–708.

Huber, W., Carey, V.J., Gentleman, R., Anders, S., Carlson, M., Carvalho, B.S., Bravo, H.C., Davis, S., Gatto, L., Girke, T., et al. (2015). Orchestrating high-throughput genomic analysis with Bioconductor. Nat. Methods *12*, 115–121.

Ivey, K.N., and Srivastava, D. (2010). MicroRNAs as regulators of differentiation and cell fate decisions. Cell Stem Cell *7*, 36–41.

Janiszewska, M., Suvà, M.L., Riggi, N., Houtkooper, R.H., Auwerx, J., Clément-Schatlo, V., Radovanovic, I., Rheinbay, E., Provero, P., and Stamenkovic, I. (2012). Imp2 controls oxidative phosphorylation and is crucial for preserving glioblastoma cancer stem cells. Genes Dev. *26*, 1926–1944.

Jønson, L., Christiansen, J., Hansen, T.V.O., Vikeså, J., Yamamoto, Y., and Nielsen, F.C. (2014). IMP3 RNP safe houses prevent miRNA-directed HMGA2 mRNA decay in cancer and development. Cell Rep. *7*, 539–551.

Kreso, A., and Dick, J.E. (2014). Evolution of the cancer stem cell model. Cell Stem Cell *14*, 275–291.

Langmead, B., Trapnell, C., Pop, M., and Salzberg, S.L. (2009). Ultrafast and memory-efficient alignment of short DNA sequences to the human genome. Genome Biol. *10*, R25.

Lee, Y., Jeon, K., Lee, J.-T., Kim, S., and Kim, V.N. (2002). MicroRNA maturation: stepwise processing and subcellular localization. EMBO J. *21*, 4663–4670.

Livak, K.J., and Schmittgen, T.D. (2001). Analysis of relative gene expression data using real-time quantitative PCR and the 2(-Delta Delta C(T)) Method. Methods *25*, 402–408.

Melo, S.A., Moutinho, C., Ropero, S., Calin, G.A., Rossi, S., Spizzo, R., Fernandez, A.F., Davalos, V., Villanueva, A., Montoya, G., et al. (2010). A genetic defect in exportin-5 traps precursor microRNAs in the nucleus of cancer cells. Cancer Cell *18*, 303–315.

Nguyen, L.H., Robinton, D.A., Seligson, M.T., Wu, L., Li, L., Rakheja, D., Comerford, S.A., Ramezani, S., Sun, X., Parikh, M.S., et al. (2014). Lin28b is sufficient to drive liver cancer and necessary for its maintenance in murine models. Cancer Cell *26*, 248–261.

Nielsen, J., Christiansen, J., Lykke-Andersen, J., Johnsen, A.H., Wewer, U.M., and Nielsen, F.C. (1999). A family of insulin-like growth factor II mRNA-binding proteins represses translation in late development. Mol. Cell. Biol. *19*, 1262–1270.

Nishino, J., Kim, I., Chada, K., and Morrison, S.J. (2008). Hmga2 promotes neural stem cell self-renewal in young but not old mice by reducing p16Ink4a and p19Arf Expression. Cell *135*, 227–239.

Nishino, J., Kim, S., Zhu, Y., Zhu, H., and Morrison, S.J. (2013). A network of heterochronic genes including Imp1 regulates temporal changes in stem cell properties. eLife *2*, e00924.

Parker, R., and Sheth, U. (2007). P bodies and the control of mRNA translation and degradation. Mol. Cell *25*, 635–646.

Pasquinelli, A.E., Reinhart, B.J., Slack, F., Martindale, M.Q., Kuroda, M.I., Maller, B., Hayward, D.C., Ball, E.E., Degnan, B., Müller, P., et al. (2000). Conservation of the sequence and temporal expression of let-7 heterochronic regulatory RNA. Nature *408*, 86–89.

Patel, A.P., Tirosh, I., Trombetta, J.J., Shalek, A.K., Gillespie, S.M., Wakimoto, H., Cahill, D.P., Nahed, B.V., Curry, W.T., Martuza, R.L., et al. (2014). Single-cell RNA-seq highlights intratumoral heterogeneity in primary glioblastoma. Science *344*, 1396–1401.

Polesskaya, A., Cuvellier, S., Naguibneva, I., Duquet, A., Moss, E.G., and Harel-Bellan, A. (2007). Lin-28 binds IGF-2 mRNA and participates in skeletal myogenesis by increasing translation efficiency. Genes Dev. *21*, 1125–1138.

Rheinbay, E., Suvà, M.L., Gillespie, S.M., Wakimoto, H., Patel, A.P., Shahid, M., Oksuz, O., Rabkin, S.D., Martuza, R.L., Rivera, M.N., et al. (2013). An aberrant transcription factor network essential for Wnt signaling and stem cell maintenance in glioblastoma. Cell Rep. *3*, 1567–1579.

Robinson, M.D., McCarthy, D.J., and Smyth, G.K. (2010). edgeR: a Bioconductor package for differential expression analysis of digital gene expression data. Bioinformatics *26*, 139–140.

Schraivogel, D., Weinmann, L., Beier, D., Tabatabai, G., Eichner, A., Zhu, J.Y., Anton, M., Sixt, M., Weller, M., Beier, C.P., and Meister, G. (2011). CAMTA1 is a novel tumour suppressor regulated by miR-9/9* in glioblastoma stem cells. EMBO J. *30*, 4309–4322.

Sen, G.L., and Blau, H.M. (2005). Argonaute 2/RISC resides in sites of mammalian mRNA decay known as cytoplasmic bodies. Nat. Cell Biol. *7*, 633–636.

Shenoy, A., Danial, M., and Blelloch, R.H. (2015). Let-7 and miR-125 cooperate to prime progenitors for astrogliogenesis. EMBO J. *34*, 1180–1194.

Shyh-Chang, N., and Daley, G.Q. (2013). Lin28: primal regulator of growth and metabolism in stem cells. Cell Stem Cell *12*, 395–406.

Shyh-Chang, N., Zhu, H., Yvanka de Soysa, T., Shinoda, G., Seligson, M.T., Tsanov, K.M., Nguyen, L., Asara, J.M., Cantley, L.C., and Daley, G.Q. (2013). Lin28 enhances tissue repair by reprogramming cellular metabolism. Cell *155*, 778–792.

Singh, S.K., Clarke, I.D., Terasaki, M., Bonn, V.E., Hawkins, C., Squire, J., and Dirks, P.B. (2003). Identification of a cancer stem cell in human brain tumors. Cancer Res. *63*, 5821–5828.

Stöhr, N., and Hüttelmaier, S. (2012). IGF2BP1: a post-transcriptional "driver" of tumor cell migration. Cell Adhes. Migr. *6*, 312–318.

Suvà, M.L., Rheinbay, E., Gillespie, S.M., Patel, A.P., Wakimoto, H., Rabkin, S.D., Riggi, N., Chi, A.S., Cahill, D.P., Nahed, B.V., et al. (2014). Reconstructing and reprogramming the tumor-propagating potential of glioblastoma stem-like cells. Cell *157*, 580–594.

Takahashi, R.-U., Miyazaki, H., and Ochiya, T. (2014). The role of microRNAs in the regulation of cancer stem cells. Front. Genet. *4*, 295.

Trapnell, C., Pachter, L., and Salzberg, S.L. (2009). TopHat: discovering splice junctions with RNA-Seq. Bioinformatics *25*, 1105–1111.

van Kouwenhove, M., Kedde, M., and Agami, R. (2011). MicroRNA regulation by RNA-binding proteins and its implications for cancer. Nat. Rev. Cancer *11*, 644–656.

Visvader, J.E. (2011). Cells of origin in cancer. Nature *469*, 314–322.

Viswanathan, S.R., Daley, G.Q., and Gregory, R.I. (2008). Selective blockade of microRNA processing by Lin28. Science *320*, 97–100.

Viswanathan, S.R., Powers, J.T., Einhorn, W., Hoshida, Y., Ng, T.L., Toffanin, S., O'Sullivan, M., Lu, J., Phillips, L.A., Lockhart, V.L., et al. (2009). Lin28 promotes transformation and is associated with advanced human malignancies. Nat. Genet. *41*, 843–848.

Wakimoto, H., Mohapatra, G., Kanai, R., Curry, W.T., Jr., Yip, S., Nitta, M., Patel, A.P., Barnard, Z.R., Stemmer-Rachamimov, A.O., Louis, D.N., et al. (2012). Maintenance of primary tumor phenotype and genotype in glioblastoma stem cells. Neuro-oncol. *14*, 132–144.

Xue, Y., Ouyang, K., Huang, J., Zhou, Y., Ouyang, H., Li, H., Wang, G., Wu, Q., Wei, C., Bi, Y., et al. (2013). Direct conversion of fibroblasts to neurons by reprogramming PTB-regulated microRNA circuits. Cell *152*, 82–96.

Yu, J.H., Yang, W.-H., Gulick, T., Bloch, K.D., and Bloch, D.B. (2005). Ge-1 is a central component of the mammalian cytoplasmic mRNA processing body. RNA *11*, 1795–1802.

Yu, F., Yao, H., Zhu, P., Zhang, X., Pan, Q., Gong, C., Huang, Y., Hu, X., Su, F., Lieberman, J., and Song, E. (2007). let-7 regulates self renewal and tumorigenicity of breast cancer cells. Cell *131*, 1109–1123.

Yu, K., Shin, J., Kim, J., Koog, M.G., Lee, J.Y., and Choi, S.W. (2015). Rapid and efficient direct conversion of human adult somatic cells into neural stem cells by article rapid and efficient direct conversion of human adult somatic cells into neural stem cells by HMGA2/let-7b. Cell Rep. *10*, 441–452.

Zhu, H., Shyh-Chang, N., Segrè, A.V., Shinoda, G., Shah, S.P., Einhorn, W.S., Takeuchi, A., Engreitz, J.M., Hagan, J.P., Kharas, M.G., et al.; DIAGRAM Consortium; MAGIC Investigators (2011). The Lin28/let-7 axis regulates glucose metabolism. Cell *147*, 81–94.